Petroleum Science 21 (2024) 519–534

Contents lists available at ScienceDirect

Petroleum Science

journal homepage: www.keaipublishing.com/en/journals/petroleum-science

Original Paper

CO_2 flooding in shale oil reservoir with radial borehole fracturing for CO_2 storage and enhanced oil recovery

Jia-Cheng Dai [a], Tian-Yu Wang [a, *], Jin-Tao Weng [a], Kang-Jian Tian [a], Li-Ying Zhu [b], Gen-Sheng Li [a]

[a] State Key Laboratory of Petroleum Resources and Prospecting, China University of Petroleum, Beijing, 102249, China
[b] China National Oil and Gas Exploration and Development Company Limited, Beijing, 100034, China

ARTICLE INFO

Article history:
Received 29 December 2022
Received in revised form
23 March 2023
Accepted 29 August 2023
Available online 30 August 2023

Edited by Jia-Jia Fei

Keywords:
Shale oil
Radial borehole fracturing
Embedded discrete fracture model
Enhanced oil recovery
Carbon storage

ABSTRACT

This study introduces a novel method integrating CO_2 flooding with radial borehole fracturing for enhanced oil recovery and CO_2 underground storage, a solution to the limited vertical stimulation reservoir volume in horizontal well fracturing. A numerical model is established to investigate the production rate, reservoir pressure field, and CO_2 saturation distribution corresponding to changing time of CO_2 flooding with radial borehole fracturing. A sensitivity analysis on the influence of CO_2 injection location, layer spacing, pressure difference, borehole number, and hydraulic fractures on oil production and CO_2 storage is conducted. The CO_2 flooding process is divided into four stages. Reductions in layer spacing will significantly improve oil production rate and gas storage capacity. However, serious gas channeling can occur when the spacing is lower than 20 m. Increasing the pressure difference between the producer and injector, the borehole number, the hydraulic fracture height, and the fracture width can also increase the oil production rate and gas storage rate. Sensitivity analysis shows that layer spacing and fracture height greatly influence gas storage and oil production. Research outcomes are expected to provide a theoretical basis for the efficient development of shale oil reservoirs in the vertical direction.

1. Introduction

With the progression of conventional reservoirs to advanced stages, marked by high-water cut (Abdel-Ghany et al., 2011), the dwindling of traditional oil reserves necessitates the search for alternative oil sources to meet burgeoning energy demands. Shale oil, a type of unconventional oil, has elicited considerable attention worldwide within the oil and gas exploration and development sectors (Zou et al., 2015). Shale oil, accounting for 20%–50% of global oil reserves, is widely distributed and estimated to have a global technically recoverable reserve of roughly 4.69×10^{10} t (Zhao et al., 2018). Nevertheless, a major challenge in shale oil reservoir exploitation is the diminished production rate due to its low and ultra-low permeability (Du et al., 2019). Therefore, hydraulic fracturing becomes crucial for shale oil production as it facilitates the extraction of oil and natural gas from challenging shale rock formations.

A horizontal well coupled with multistage fracturing that proficiently engenders a fracture network within target strata is a commonly employed technique to ameliorate shale reservoir properties, accelerate oil mobility, and boost oil recovery (Boak and Kleinberg, 2020). Yet, the deployment of this technology is hindered by limited fracturing performance and elevated operational costs per well (Yang et al., 2019; Wang et al., 2021). For instance, in 2019, Jimsar shale oil in Xinjiang incurred 61 million RMB in drilling and fracturing expenses, leading to a deficit in total revenue (Lei et al., 2021). Concurrently, the layered structure of these formations exhibits substantial variations in vertical and horizontal permeability ($K_v/K_h = 10^{-2}$ to 10^{-3}), thereby reducing the degree of exploitation in the vertical direction of shale reservoirs (Sun et al., 2021; Hu et al., 2020). Furthermore, layered strata could limit the vertical extension of fractures, resulting in constrained fracture height (Tang et al., 2019; Li et al., 2020). For example, recorded fracture heights in the Eagle Ford shale oil reservoir are typically lower than 30–40 ft, substantially less than the reservoir thickness (Simpson et al., 2016). Consequently, an innovative approach that can enhance the stimulated reservoir volume (SRV), curb drilling

* Corresponding author.
E-mail address: wangty@cup.edu.cn (T.-Y. Wang).

https://doi.org/10.1016/j.petsci.2023.08.033

and fracturing expenses, and improve economic viability is critically needed.

Radial borehole fracturing, emerging as a novel reservoir stimulation technique, offers an economical alternative and supplement to horizontal well fracturing due to its lower operational costs (Dai et al., 2023b; Gong et al., 2016). Prior to hydraulic fracturing, several laterals, each measuring 30–50 mm in diameter and spanning a length of 50–100 m, are drilled utilizing high-pressure jets (Huang and Huang, 2019). These laterals, which can be drilled across multiple layers along a vertical well, serve as conduits for fracturing fluid to stimulate the inception and propagation of fractures, thus creating a fracture network (Liu et al., 2018). As such, hydraulic fractures can be established in strata at varying depths, providing a tangible solution to the issue of confined vertical SRV in horizontally oriented fractures (Yang et al., 2022). To date, there have been successful applications of this technology in several countries including China, the United States, and Russia (Cinelli and Kamel, 2013; Li et al., 2000; Novokreshchennykh and Raspopov, 2016). One of the notable examples is in the Tarim Oilfield, China, where well KC1, post-radial borehole fracturing, exhibited a threefold increase in productivity (Teng et al., 2014).

Radial boreholes can modify formation stress, significantly lowering the fracture initiation pressure relative to perforation-induced fracturing (Yan et al., 2017; Guo et al., 2017; Wang et al., 2020). Experimental research conducted by Tian et al. (2019) revealed that the peak pressure of radial borehole fracturing is merely 1/4 to 1/3 of that exerted by traditional hydraulic fracturing. Concurrently, it demonstrated fracturing performance 1.38 to 7.07 times superior to the conventional approach, effectively boosting fracture propagation. Bai et al. (2021) established that formation stress accumulates near radial boreholes, facilitating rock fragmentation and expedited fracture propagation. Guo et al.'s laboratory tests (Guo et al., 2022) found that stress variations near radial boreholes depend on the spatial arrangement of multiple boreholes, impacting the fracture propagation rate and performance. Wang et al. (2020) concluded that the breakdown pressure could be effectively mitigated when the radial borehole number exceeds three. Radial boreholes also serve to manage and steer fractures, thus promoting fracture expansion and propagation. Tian et al. (2017) posited the existence of a plastic zone around the radial borehole, where induced fractures propagate directionally, unhindered by formation stress. Li et al. (2019) determined, via numerical simulation, that stress developed during the drilling process directs the radial propagation of fractures up to an effective distance of 40 m.

The swift decline in pressure and production rate poses a challenge in the process of shale oil production. Given the micro and nanopores in shale formations, conventional water flooding techniques offer limited effectiveness in sustaining the production rate. CO_2 flooding, on the other hand, emerges as an enhanced oil recovery (EOR) technology that is well-suited to shale reservoirs (Lan et al., 2021; Sheng, 2015; Zhu et al., 2019). The abundant micro and nanopores within shale reservoirs accelerate CO_2 capture and storage during the diffusivity process (Bacon et al., 2015), effectively addressing the issue of inadequate fluid mobility. Optimal performance is achieved when CO_2 is in a miscible state (Li et al., 2017; Song and Yang, 2017). The migration of CO_2 through fractures gradually increases the contact area between gas and oil, which further expands with the number of fractures in the reservoir, paralleling the oil recovery rate. Field tests by Sorensen et al. (2018) demonstrated that hydraulically fractured shale reservoirs can store 26% more CO_2 compared to undeveloped shale reservoirs. Gamadi et al. (2013) concluded that circulating CO_2 injection into shale can effectively elevate shale oil recovery by 33%–85%. Jin et al. (2017) performed CO_2 flooding experiments on Bakken shale and found that each gram of shale captured 17 mg of CO_2, with the EOR degree by using CO_2 ranging from 15% to 65%. Similar results were simulated by Huang et al. (2020), who found that injecting CO_2 into low-permeability shale gas reservoirs can enhance gas recovery and store 10%–20% of CO_2 within the formation. Additionally, CO_2 flooding aligns with net-zero emissions or carbon neutrality goals (Zhao et al., 2022). Specifically, employing CO_2 flooding in the development of shale oil and gas reservoirs facilitates efficient CO_2 utilization and storage while amplifying oil and gas recovery rates (Cavanagh and Ringrose, 2014; Liu et al., 2017; Xie et al., 2021; Xu et al., 2019).

This paper proposes an approach where CO_2 flooding is applied to a shale reservoir post radial borehole fracturing. Herein, multiple radial boreholes at various shale reservoir layers facilitate hydraulic fracturing, followed by CO_2 injection for flooding after forming an intricate fracture network. The application of this method, as depicted in Fig. 1, involves dividing the reservoir into upper and lower layers, each containing four radial boreholes that each initiate a hydraulic fracture. CO_2 is then pumped from the surface injection pump to the main well's annulus space and penetrates the reservoir's top via the upper radial boreholes. The injected gas propels the reservoir oil from the upper to the lower layer, pushing oil flow into the tubing from the lower layer and facilitating pumping to the surface. This development technique could potentially boost reservoir utilization and CO_2 storage efficiency. Currently, the drilling and completion cost for a single horizontal well in continental shale in the United States ranges from 4.7 to 8.2 million USD (Yang et al., 2019) while the cost for a vertical well is a mere 2.5 million USD (Cui et al., 2022). Thus, this method could potentially lower the development cost of shale oil, considering that the drilling and completion cost for a vertical well amounts to only 50%–77% of a horizontal well at the same depth (Mukherjee and Economides, 1991).

In exploring the feasibility of developing shale oil reservoirs via CO_2 flooding coupled with radial borehole fracturing, this study introduces a novel methodology, predicated on the radial borehole fracture network, that employs CO_2 flooding to augment shale reservoir development efficiency and attain CO_2 storage. Leveraging the parameters of the Gulong Oilfield, the study establishes a productivity model for CO_2 flooding shale oil reservoirs

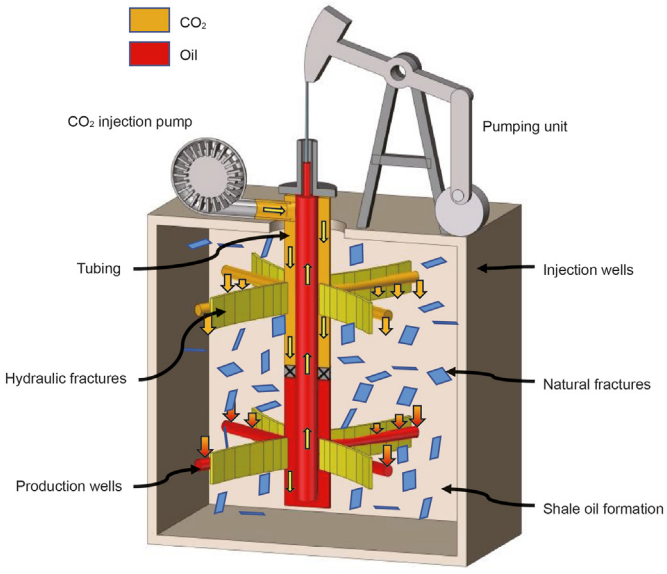

Fig. 1. CO_2 flooding with a two-layer radial fracturing structure in a vertical well.

with radial borehole fracturing, in line with the coupled matrix-fracture-wellbore flow mechanism. Following model validation through field data and a grid independence check, the study proceeds to examine the correlation between the pressure field, CO_2 saturation distribution, and time. Finally, the study conducts a sensitivity analysis on variables including injection location, layer spacing, pressure difference, borehole number, and hydraulic fractures. The anticipated research findings aim to furnish a theoretical framework for the efficient development of shale reservoirs via radial borehole fracturing.

2. Model development

2.1. Model assumptions

The understanding of fluid flow dynamics within and across the matrix, fracture, and wellbore systems is of crucial importance in the context of radial borehole fracturing within shale reservoirs. In response to this, the present study proposes a comprehensive numerical model tailored to capture the intricate flow behavior exhibited by CO_2 flooding in combination with radial borehole fracturing, taking into account both hydraulic and naturally occurring fractures. The model serves to predict oil productivity and gas storage capacity. The presumptions underpinning this model are delineated as follows:

1) The reservoir's permeability varies horizontally and vertically but maintains its single porosity.
2) Flow in the reservoir is assumed to be isothermal with negligible temperature change.
3) Natural fractures in the reservoir are symmetrical about the horizontal plane in the middle to avoid possible interference in simulating different lateral-well configurations.
4) The influence of natural fractures on the propagation of hydraulic fractures is ignored
5) The model neglects gas evolution, condensation, and wax precipitation.
6) The flooding mechanism for CO_2 to oil is miscible displacement, while declines in oil viscosity with injected CO_2 are neglected.
7) CO_2 diffusion and adsorption effect are neglected as this paper considers the main driving force of oil and gas in the reservoir to be the pressure difference between the injector and the producer.
8) Changes in the matrix, fractures, and fluid properties with pressure are neglected.
9) Possible increases in matrix permeability in the vicinity of the wellbore and potential micro-fractures associated with main hydraulic fractures are neglected. All hydraulic fractures are assumed to have identical fracture heights.

2.2. Mathematical equations

Though compositional models are typically deemed more precise in characterizing the CO_2 flooding process in shale oil reservoirs (Dai et al., 2023a; Jia et al., 2019), a black oil model is nonetheless an effective tool for conducting such simulations when data availability is limited, and faster computational speed is required (Hoffman, 2012). The present study employs a modified black oil model that incorporates three distinct phases: oil, water, and gas (CO_2), to simulate the CO_2 flooding process within the reservoir.

2.2.1. Flow in matrix

A shale reservoir is typically characterized by tight formation where fluid flow in the matrix presents non-Darcy characteristics. The exponential non-Darcy flow equation in literature (Wang and Sheng, 2017) is adopted herein. Combined with the mass conservation equation, the equation gives:

$$\nabla\left\{\lambda_\alpha\rho_\alpha\left(\frac{1}{1+ae^{-b|\nabla P_\alpha|}}\right)[\nabla(P_\alpha-\rho_\alpha gZ)]\right\}+q_\alpha^{nnc}+q_\alpha^{w}=\frac{\delta}{\delta t}(\varphi\rho_\alpha S_\alpha) \tag{1}$$

where the subscript α represents one of the phases among oil, water, gas (CO_2 in this case); λ_α represents phase mobility in D/(Pa·s); P_α represents phase pressure in Pa; ρ_α represents phase formation density in kg/m^3; g is the gravitational acceleration, being 9.8 N/kg; Z is depth in m; S_α is phase saturation; φ refers to porosity and t refers to the time in s; q_α^{nnc} and q_α^{w} refer to coupling terms between matrix, fractures, and the wellbore, expressed in kg/(m^3·s); the dimensionless coefficient a and b in the non-Darcy term can be expressed as the functions related to phase mobility λ_α:

$$a=-0.6095\lambda_\alpha{}^3+2.5821\lambda_\alpha{}^2-3.4594\lambda_\alpha+1.5836 \tag{2}$$

$$b=0.3603\lambda_\alpha{}^2-0.1049\lambda_\alpha+1.0935 \tag{3}$$

2.2.2. Flow across fractures, matrix, and within fractures

Key to simulating post-fracturing productivity has been the successful treatment and coupling of hydraulic fractures. Various models such as dual-porosity, dual-permeability, or a combination of both, can effectively couple the organic and inorganic pores within the shale reservoir. Moreover, they accurately depict the flow relationship between the stimulated and unstimulated zones by incorporating the interplay between fractures and matrix. Nevertheless, the Embedded Discrete Fractures model (EDFM) presents an advantage in its ability to simulate more complex fracture geometries. The EDFM diminishes the flow dimension within fractures to one level lower than that of reservoirs, thus establishing an autonomous fracture flow system (Dachanuwattana et al., 2018; Liu et al., 2021). As fractures typically emerge in post-fracturing phase of shale reservoirs, the present study utilizes the EDFM to reduce the dimensionality of hydraulic fractures. Herein, three-dimensional fractures are simplified into multiple planar interfaces within the matrix grids. The Navier-Stokes equation governs flows within these fractures and can be equivalently represented by Darcy's flow (Kim and Deo, 2000; Lee et al., 2000, 2001). These flows are subsequently discretized using the Two-point Flux Approximation method (TPFA).

In the EDFM, flow across fractures, matrix, and within fractures (the coupling term in Eq. (1)), is uniformly expressed as:

$$q_\alpha^{NNC}=\rho_\alpha\lambda_\alpha T_{NNC}\Delta P_\alpha \tag{4}$$

where T_{NNC} refers to the transmissibility between any non-neighboring connected units, expressed in D·m. The non-neighboring connection units are the units that are physically connected through grids and nodes but are not adjacent to each other in turns of computing grids. The T_{NNC} can be expressed as:

$$T_{NNC}=\frac{k_{NNC}A_{NNC}}{d_{NNC}} \tag{5}$$

where k_{NNC}, A_{NNC}, and d_{NNC} represent the permeability, contact area, and distance between non-neighboring connected units, respectively in D, m^2, and m. The expressions of k_{NNC}, A_{NNC}, and d_{NNC} are different in terms of connection types between different

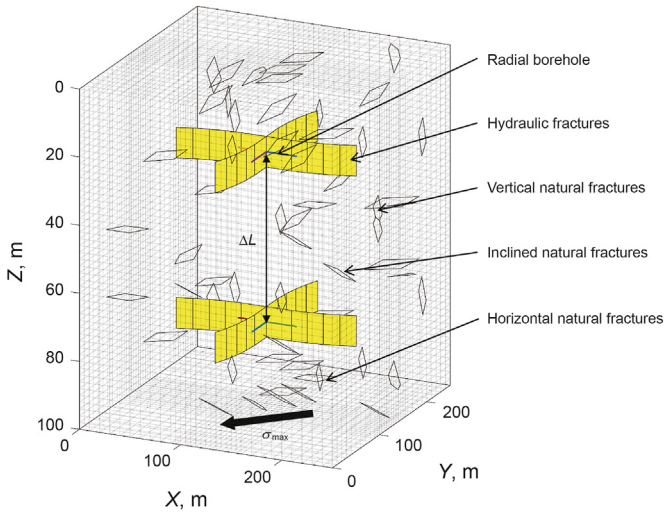

Fig. 2. Distribution of hydraulic and natural fractures after radial borehole fracturing.

units, and have been illustrated in detail in the literature (Xu, 2015).

2.2.3. Flow within radial boreholes, between boreholes, matrix, and fractures

Flow within radial boreholes is treated as one-dimensional flow, with mass conservation equation expressed as:

$$\frac{\partial}{\partial t}(x_\alpha \rho_\alpha) + \frac{\partial}{\partial x}(v_\alpha) - q_\alpha^{\mathrm{w}} = 0 \tag{6}$$

where x_α refers to dimensionless phase volume fraction.

The coupling relations of flow across borehole, matrix, and fractures can be expressed as:

$$q_\alpha^{\mathrm{w}} = J_{\mathrm{w}} \lambda_\alpha \rho_\alpha [P_{\mathrm{bh}} - P_\alpha - \rho_\alpha g \Delta Z] \tag{7}$$

Table 2
Fluid parameters of CO_2.

Fluid	CO_2 density, kg·m^3	CO_2 compressibility	CO_2 viscosity,Pa·s
CO_2 at 20 MPa	510.9848	5.1425e-08	3.9152e-05
CO_2 at 30 MPa	686.5266	1.7015e-08	5.6830e-05
CO_2 at 40 MPa	776.4407	9.0714e-09	6.9591e-05
Brine	1000	1.0000e-13	1.0000e-03
Oil	700	1.0000e-10	7.0000e-04

where P_{bh} represents radial borehole pressure, Pa; J_{w} refers to the well index in m^3/(s·Pa), which represents the potential or ability of a well to produce. In the Cartesian coordinate system, the well index for borehole-matrix can be expressed as (Peaceman, 1983):

$$J_{\mathrm{w}} = \frac{\theta k h}{\ln(r_{\mathrm{e}}/r_{\mathrm{w}}) + S} \tag{8}$$

where kh is the product of effective permeability and net thickness, in D·m; r_{w} represents wellbore radius, in m, and r_{e} is the equivalent radius, in m; S is the dimensionless skin factor; the dimensionless coefficient θ changes with respect to the coupling relations between wellbore and matrix. The well index for borehole-fracture can be expressed as (Moinfar et al., 2013):

$$J_{\mathrm{f}} = \frac{2\pi k_{\mathrm{f}} w_{\mathrm{f}}}{\ln(r_{\mathrm{e}}/r_{\mathrm{w}})} \tag{9}$$

The discretization of governing equations for flows in matrix, wellbore, and fractures can be expressed by the Newton-Raphson iterative method:

$$\frac{\partial R^{n+1}}{\partial X}\Delta X = -R^{n+1} \tag{10}$$

where the term on the left side is the Jacobian matrix, with X being the initial variable, n indicates the previous time step.

In this paper, Eq. (10) is solved based on MATLAB Reservoir Simulation Toolkit (MRST) (Lie, 2019; Lie and Møyner, 2021). MRST

Table 1
Shale reservoir parameters.

Parameters	Values	Parameters	Values
Matrix vertical permeability	0.0001 mD	Hydraulic fracture porosity	80%
Matrix horizontal permeability	0.58 mD	Hydraulic fracture conductivity	10^3 D·cm
Matrix porosity	6.20%	Natural fracture porosity	80%
Initial reservoir pressure	31.6 MPa	Natural fracture conductivity	10 D·cm
Initial reservoir temperature	94.0 °C		

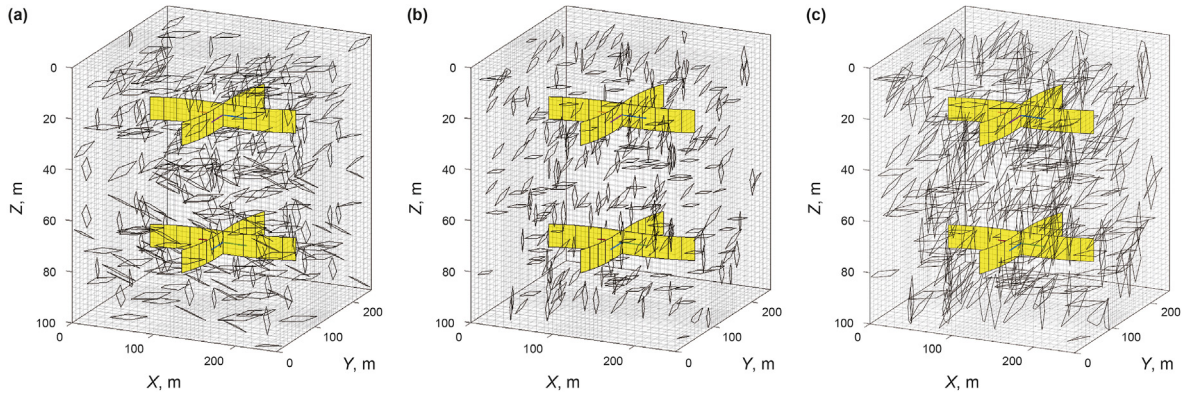

Fig. 3. Diagram of natural fracture distribution: (**a**) symmetrical natural fracture, (**b**) asymmetric natural fracture, (**c**) asymmetric natural fracture with enlarged area.

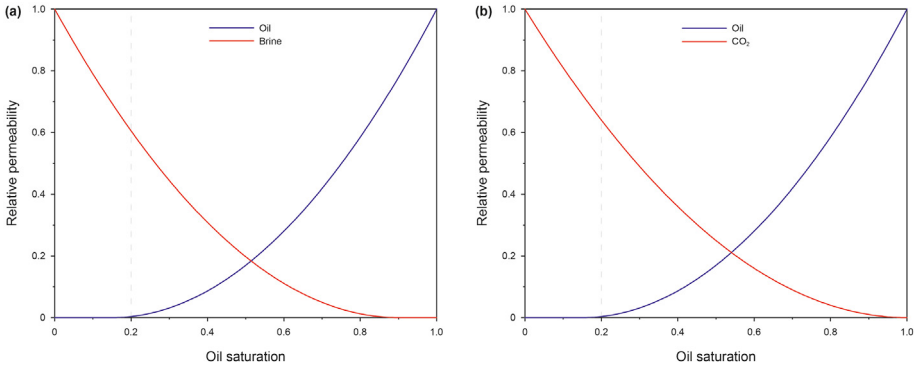

Fig. 4. Relative permeability curves: (**a**) oil-brine relative permeability, (**b**) oil-gas relative permeability.

Table 3
Parameters of radial borehole fracturing.

Parameters	Basic values	Range	Unit
Interlayer spacing	50	10 to 60	m
Pressure difference	20	10 to 49	MPa
Borehole number	4	1 to 4	-
Fracture height	9	1 to 19 (Zeng et al., 2022)	m
Fracture length	100	50 to 150 (Sheng and Chen, 2014)	m

is an open-access reservoir modeling and numerical simulation software. It provides a comprehensive black oil and compositional reservoir simulator capable of simulating industry-standard models and includes a graphical user interface for post-processing simulation results.

After calculation, oil production rate (t/d) and cumulative oil production (t) are selected as indicators to measure oil productivity. Meanwhile, to measure reservoir CO_2 storage capacity, two indicators, the CO_2 storage rate (m^3/d) and the accumulated CO_2 storage amount (m^3), are selected, which can be expressed as follows:

$$CO_2 \text{ storage rate} = CO_2 \text{ injection rate} - CO_2 \text{ production rate} \tag{11}$$

$$CO_2 \text{ storage capacity} = \text{cumulative } CO_2 \text{ injection} - \text{cumulative } CO_2 \text{ production} \tag{12}$$

To further characterize the storage efficiency of injected CO_2, define R_g as the ratio of the CO_2 production rate over the CO_2 injection rate:

$$R_g = \frac{CO_2 \text{ production rate}}{CO_2 \text{ injection rate}} \tag{13}$$

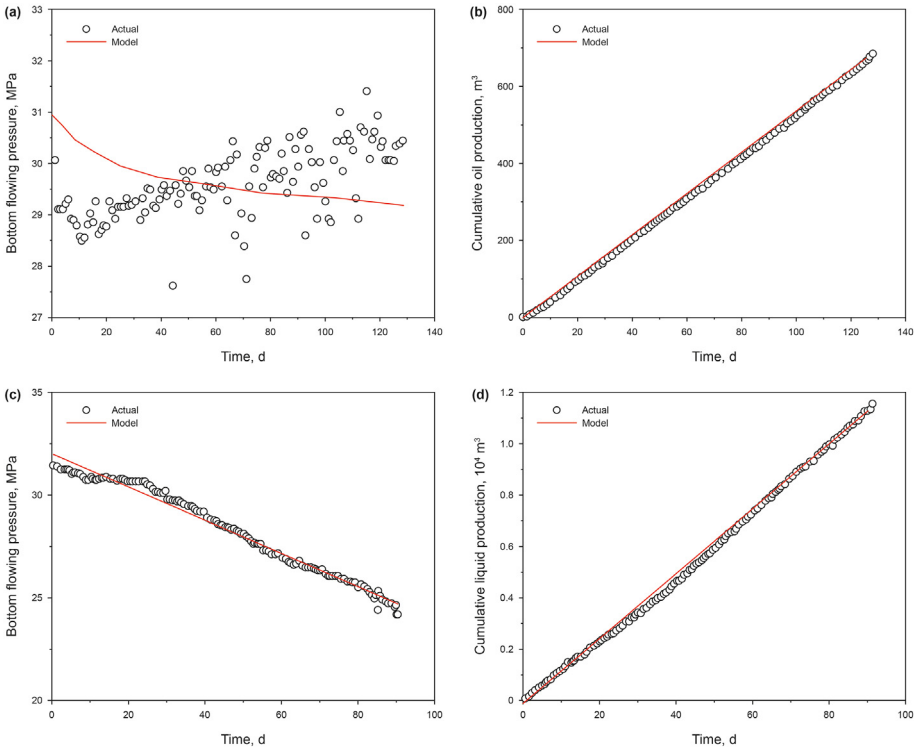

Fig. 5. Calculated and measured data: (**a**) bottom flowing pressure of well CP-1, (**b**) cumulative oil production of well CP-1, (**c**) bottom flowing pressure of well A-1, (**d**) cumulative liquid production of well A-1.

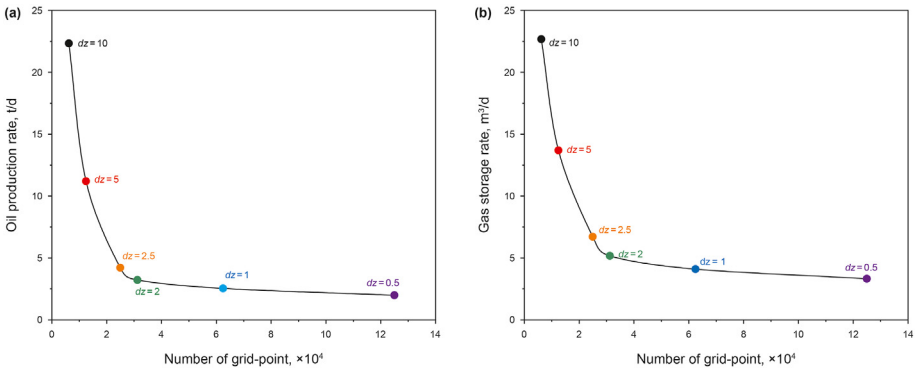

Fig. 6. Effect of the number of grid-point to (**a**) oil storage rate and (**b**) grid number.

An R_g closer to 1 means a lower gas storage effect. Similarly, to characterize CO_2 flooding efficiency, define R_o as the ratio of CO_2 injection rate over oil production rate, which is the volume of CO_2 needed to be injected to produce a unit volume of oil:

$$R_o = \frac{CO_2 \text{ injection rate}}{\text{Oil production rate}} \tag{14}$$

A higher R_o indicates a lower efficiency in CO_2 displacement.

3. A multilateral well fracturing case

3.1. Computational model

The computational model for the shale reservoir, as presented in Fig. 2, encompasses surrounding rock, an upper injection well, a lower production well, hydraulic fractures oriented by radial boreholes, and natural fractures. The reservoir model spans 250 m × 250 m × 100 m and resides at depths between 2000 and 2500 m. Table 1 delineates the pore and permeability characteristics of the reservoir and fractures. As shale reservoirs are characteristically well-laminated and layered, the vertical permeability is considerably lower than the horizontal permeability while the porosity remains uniform. Furthermore, to distinguish between hydraulic and natural fractures, the conductivity of the latter is set at 1% of that of hydraulic fractures. A closed boundary condition is employed, which positions the injector as the exclusive source of pressure. The radial borehole extends to a length of 30 m and has a radius of 15 mm. In the base case scenario, two strata of radial wells are present, separated by a 50 m spacing between the upper injection well and the lower production well. Each stratum accommodates four radial boreholes, which are arranged orthogonally to each other, with the radial wells in both strata following identical orientations.

The geometric details of the hydraulic fractures can be found in the Appendix. The open-source software Alghalandis Discrete Fracture Network Engineering (ADFNE) (Alghalandis, 2017) is employed to generate rhombuses that serve as proxies for natural fractures. Fig. 3(a) illustrates that the base case comprises three sets of natural fractures, with 0°, 90°, and 45° planes symmetrically aligned with respect to the horizontal plane at $dz = 50$ and 100 m for each type. The length of these natural fractures falls within the 20–30 m range, while the orientation of each fracture type ranges from 35° to 55°. Although the number of fractures depicted in Fig. 3(b) remains consistent, their distribution is randomized. Fig. 3(c) presents a scenario wherein the fracture area is twice that of Fig. 3(b). The natural fractures featured in Fig. 3(b) and (c) are incorporated only in discussions pertaining to the direction of CO_2

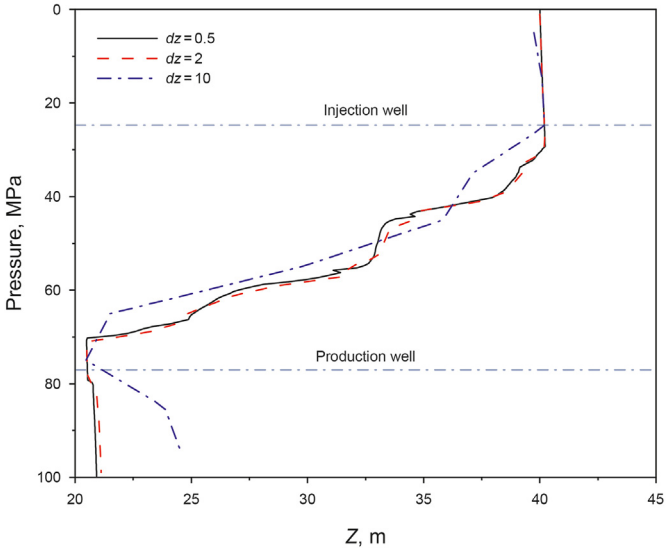

Fig. 7. Pressure distribution in the mid-axis of the reservoir *x-y* plane.

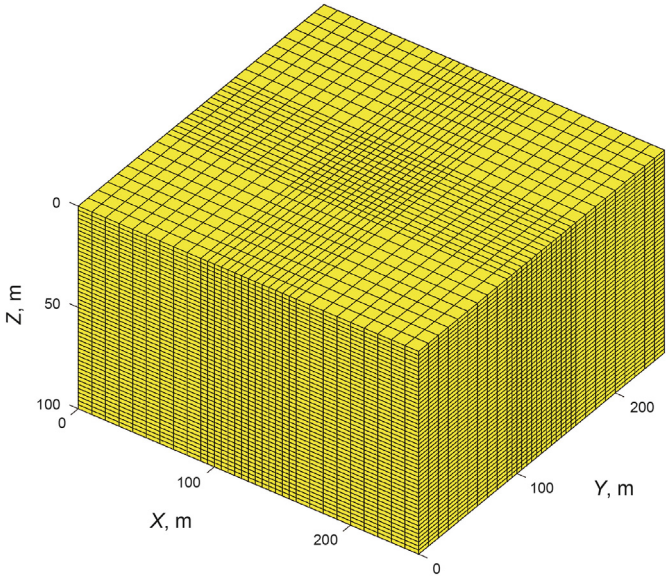

Fig. 8. Schematic of the numerical reservoir simulation grids.

injection.

The initial pressure of the reservoir is set to 31.6 MPa, with an initial oil saturation of 60%, a residual oil saturation of 15%, and a connate water saturation of 10%. The injection pressure is maintained at 40 MPa, while the production pressure is kept at 20 MPa. These pressures ensure that the CO_2 is in the supercritical phase, where it has a lower density and viscosity than water but exhibits higher compressibility. Simultaneously, these pressure parameters facilitate a miscible displacement type. The physical properties of CO_2, water, and oil are detailed in Table 2. The relative permeability curves of oil, water, and CO_2 are displayed in Fig. 4. In this study, the total simulation duration lasts 10 years, with a time step length of 10 days. Table 3 summarizes the parameters analyzed in this paper. The ratio of radial well spacing to reservoir layer thickness is referenced to similar applications of CO_2 flooding methods in geothermal studies (Shi et al., 2018). The number of radial wells does not exceed four because experiments have indicated that no additional fractures are generated when the number of radial wells surpasses four (Guo et al., 2022).

3.2. Model validation

To further affirm the accuracy of our proposed productivity model for fractured horizontal wells, data from two wells, CP-1 and A-1, located in the Gulong Oilfield are employed for model validation (Pang et al., 2020). These wells are representative of the reservoir, with the collected data encompassing bottom-hole flowing pressure and cumulative oil production. As depicted in Fig. 5, the calculated bottom-hole flowing pressure for both wells remain consistent with the measured data, with the maximum deviation being within 10%. This discrepancy is attributed to the turbulent production rates in the validation case. The findings substantiate the model's robustness and further corroborate its precision in predicting the production rate for the hydraulic fracturing case.

3.3. Simulation mesh

In constructing a reservoir matrix, this study employs structured grids. With a cell length and width of 10 m, the oil production and gas storage in the 10th year exhibit a decline as cell height decreases (i.e., grid number increases). As demonstrated in Fig. 6, when the cell height falls below 2 m, the diminishing trend of oil production and gas storage lessens. When the cell height is set at 0.5 m, the oil production and gas storage in the 10th year are only marginally higher than those observed at a cell height of 2 m, with increases of 1.28 t/d and 2.15 m^3/d respectively.

Fig. 7 depicts the variation of reservoir pressure along the axis for three different grid sizes in the z-direction (dz = 10, 2, and 0.5 m). The findings reveal that larger grid sizes hinder the simulation's ability to accurately capture the pressure gradient. This leads to significant local pressure gradients near the CO_2 injection well and production well, causing the gas injection and oil production rates to rise. Conversely, smaller grid sizes facilitate more accurate reproduction of pressure gradients, thereby yielding more precise simulation outcomes.

In the subsequent simulation process, as oversized grids can eventually affect computational accuracy while undersized grids can lead to excessive calculation time, the grid height is set to be 2 m. At this height, the refinement of grids along horizontal direction can only exert an effect on oil production and gas storage in a very short time at the initial stage of production. Therefore, grids length and width within 35 m of the horizontal central axis of the reservoir are locally refined to 5 m, which gives the total grid number of 31,250 to study the characteristics of pressure and CO_2 saturation in the area near boreholes and hydraulic fractures, as shown in Fig. 8.

4. Results and discussions

4.1. Analysis of pressure and CO_2 saturation in reservoir

The relationship between reservoir pressure, CO_2 saturation, and time during production is the basis for improving shale

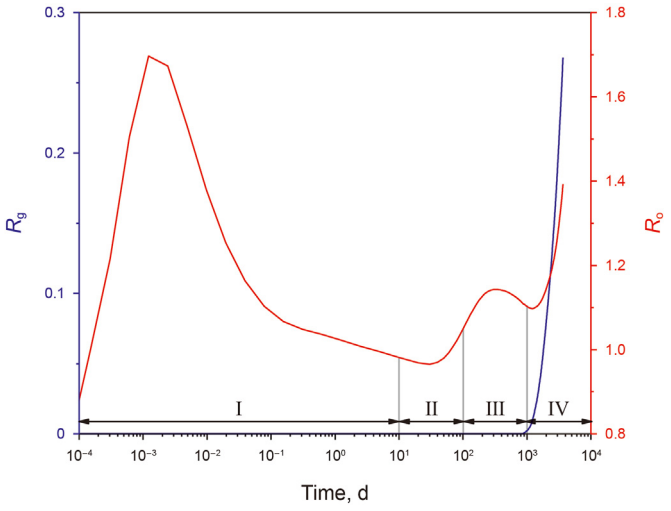

Fig. 10. R_g and R_o vs. time (I to IV represents four flowing stages).

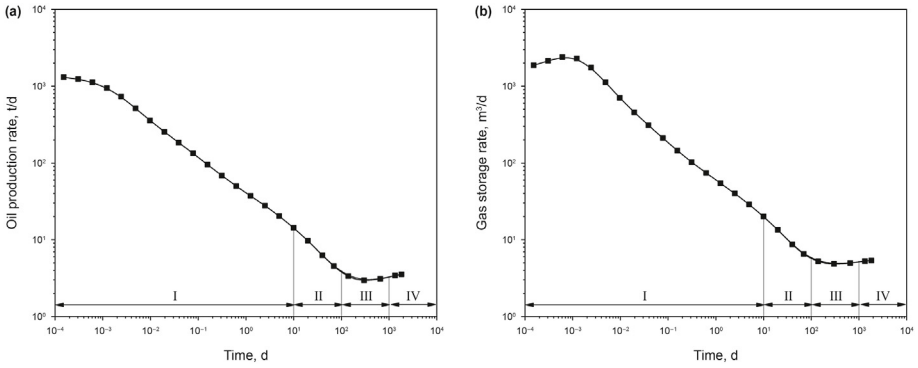

Fig. 9. Daily production/storage vs. time (**a**) oil production (**b**) gas storage. (I to IV represents four flowing stages).

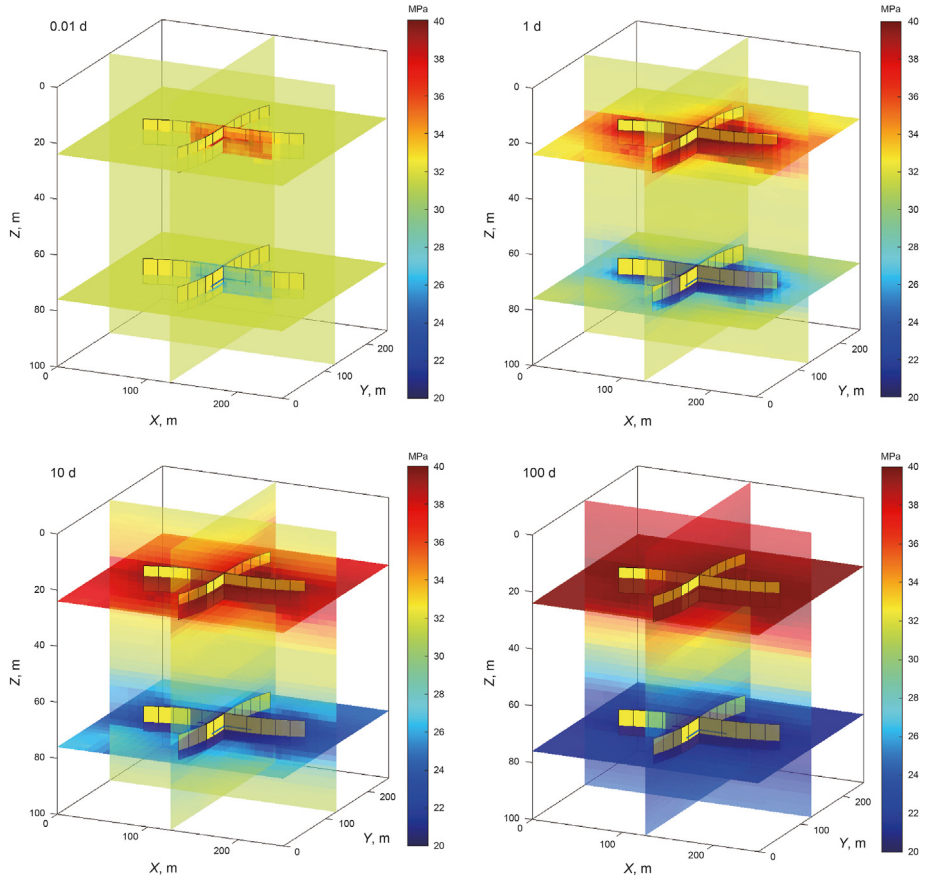

Fig. 11. Reservoir pressure distribution at 0.01, 1, 10, and 100 d.

reservoir development by CO_2 flooding with radial borehole fracturing. This study aims to understand and optimize the CO_2 flooding process for enhanced oil recovery and gas storage. The CO_2 flooding process is divided into four distinct stages based on the observed changes in oil production rate (Fig. 9(a)), gas storage rate (Fig. 9(b)), efficiency (Fig. 10), pressure (Fig. 11), and CO_2 saturation distribution (Fig. 12) with time (Bai et al., 2022). These stages were chosen as they represent critical transitions and help us better understand the underlying mechanisms that drive the process.

Stage I: This stage lasts from the initial day to the 10th day of production, where pressure propagates horizontally. A low-pressure region occurs centering the producer and its hydraulic fractures, while a high-pressure region occurs around the injector and its hydraulic fractures. Due to the large difference between vertical and horizontal permeability, an increase or depletion in pressure caused by the injector or producer propagates along the horizontal planar direction. In this stage, horizontal migrations dominate the flow of CO_2, while vertical migrations through natural fractures begin. With the release of elastic energy of rock and fluid, oil production and gas storage decrease rapidly, increasing R_o first and then decreasing. Although brief in duration, Stage I creates the highest oil production rate compared to all other stages.

Stage II: This stage follows the previous stage and lasts till the 100th day of production, where pressure difference propagates vertically. Due to the closed boundary, pressure stabilizes along the horizontal direction. The high-pressure region caused by the injector starts to spread vertically toward the producer. The region between the two wells starts to be affected and starts to form pressure gradients that gradually decline from the injector to the producer. Therefore, CO_2 migrates from the injector to the producer through natural fractures. As reservoir pressure keeps varying under pressure differences, oil production and gas storage continue to decrease. In this stage, the R_o decreases at first and then increases. The area of the horizontal plane primarily influences the duration of Stage II due to the presence of closed boundaries. Furthermore, the duration of Stage II is also impacted by factors such as the lateral number and fracture length, which are discussed in later sections of the paper.

Stage III: At this point, the reservoir reaches stabilized production and lasts from the 100th day to the 1000th day of production. In this stage, reservoir pressure stabilizes while the pressure difference between the injector and the producer maximizes, thus leading to an increase in both oil production and gas storage. CO_2 continues to migrate vertically through natural fractures. The R_o increases first and then decreases in this stage. Stage III is the most critical stage for CO_2 storage, as CO_2 has not yet been produced from the production well during this phase. Additionally, the duration of Stage III is significantly influenced by factors such as interlayer spacing, pressure difference, and fracture height, which are discussed in subsequent sections of the paper.

Stage IV: In this stage, gas channeling occurs, starting from the 1000th day to the 10th year of production. By this time, reservoir pressure remains unchanged, yet CO_2 starts to enter the producer, increasing the gas production rate and lowering the oil and gas storage rates after their peaked values. Therefore, here the occurrence of peak values in both rates marks the beginning of the gas

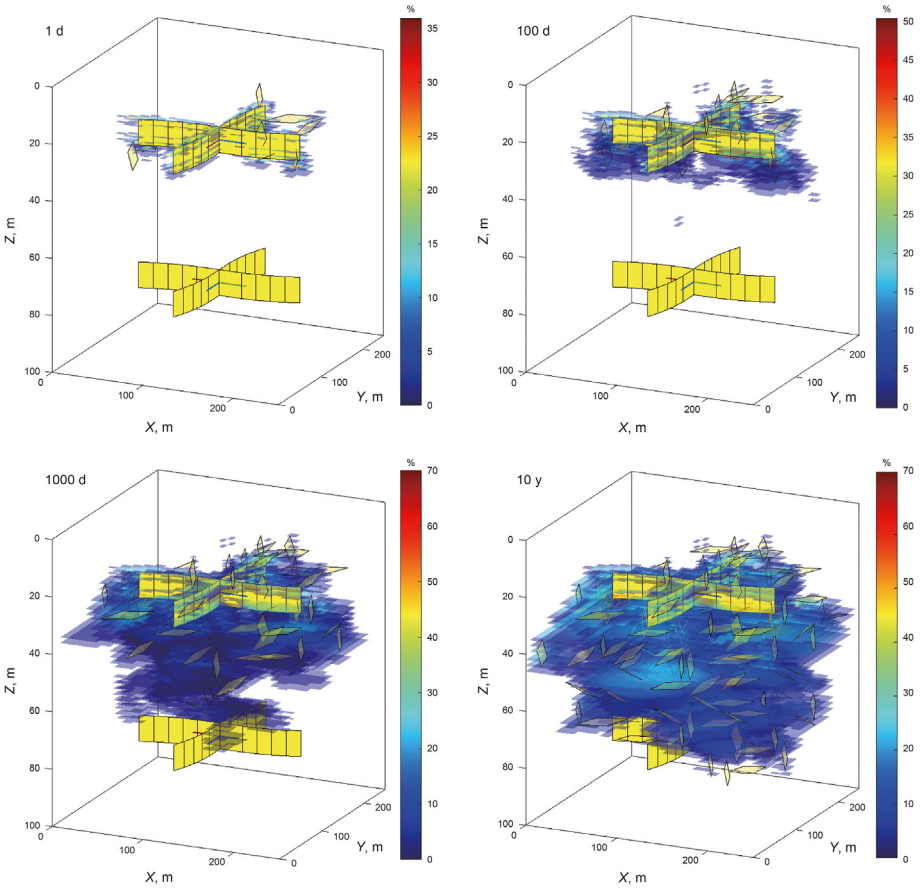

Fig. 12. CO_2 saturation distribution at 0.01, 1, 10, and 100 d: only matrix and natural cracks with CO_2 saturation greater than 5% are mapped.

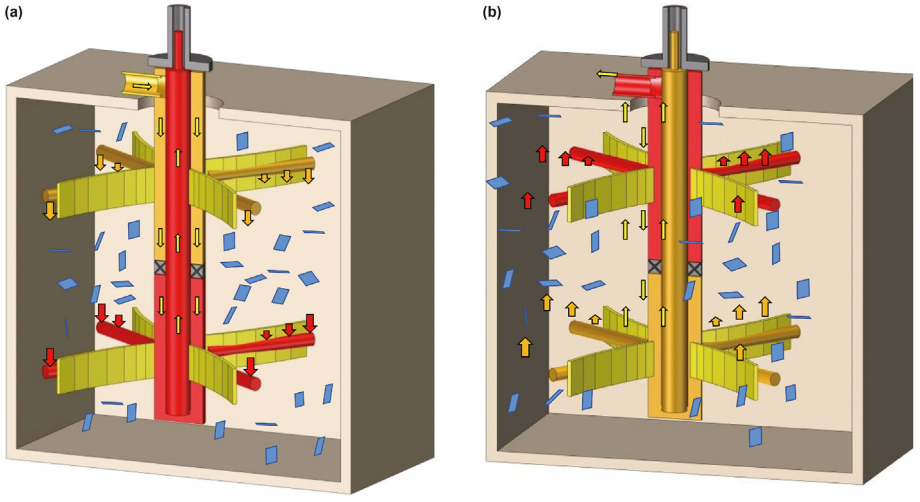

Fig. 13. Schematic of well configuration (**a**) upper injector and lower producer, (**b**) upper producer and lower injector.

channeling effect. In this stage, both R_g and R_o increase rapidly, meaning the efficiency of oil production and gas storage gradually decreases. Therefore, it may be necessary to consider halting the injection process.

4.2. Comparison of different lateral-well configurations

The chosen layer for CO_2 injection (either upper or lower) significantly determines the well configuration during the production phase. For instance, when CO_2 is injected from the lower layer, it is channeled into the reservoir's base through the main well's tubing, propelling oil to migrate from the lower to the upper layer. The oil then flows into the casing from the top of the reservoir and is subsequently transported to the surface, as illustrated in Fig. 13.

Two distinct well configurations, signifying the upper and lower

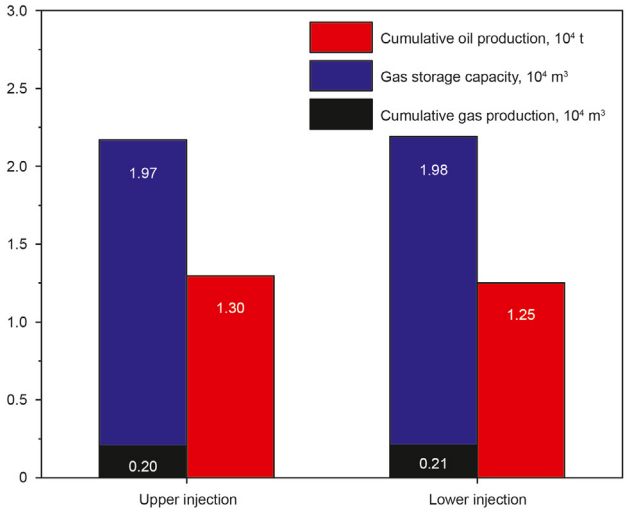

(a) Fracture I

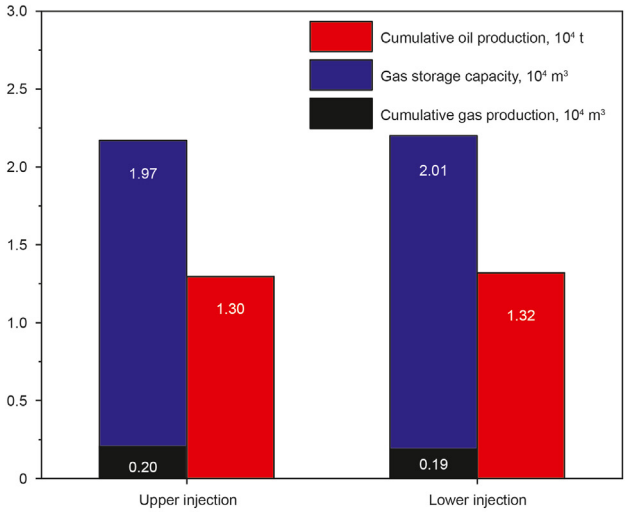

(b) Fracture II

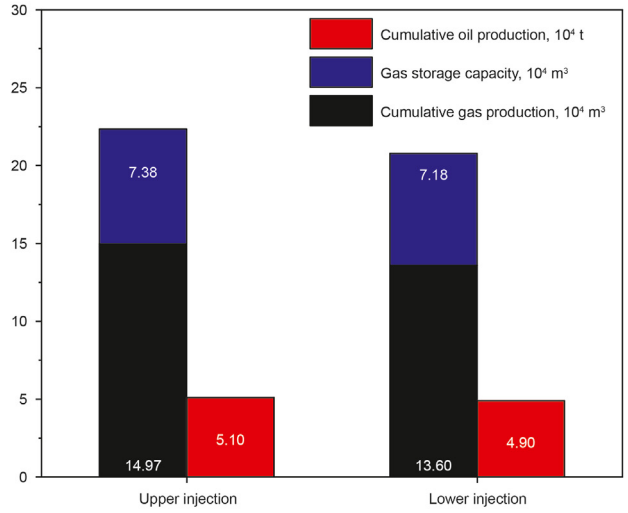

(c) Fracture III

Fig. 14. Cumulative oil production and gas storage histogram of upper injection and lower injection.

injectors, are contrasted here based on their respective productivities. According to Fig. 14(a), there is a minimal disparity in cumulative oil production and cumulative gas storage between the two scenarios by the tenth year. Notably, the cumulative oil production in the case with an upper injector exceeds that of the lower injector by 0.4×10^4 t. In contrast, the cumulative gas storage of the upper injector case is 0.1×10^4 t less than the scenario with the lower injector. This difference can be primarily attributed to the influence of gravity. When the injector is positioned above, gravity impacts the oil and drives it downward, thereby elevating the oil production rate. Conversely, in the case of a lower injector, CO_2 is inclined to ascend, culminating in greater gas storage and gas production. Fig. 14(b) depicts that when the fracture number remains unaltered, but their distribution is randomized, the magnitudes of cumulative oil production, cumulative gas production, and cumulative gas storage show small difference compared to those of the base case. This observation proves that the model can offer precise production forecasts even though symmetrically distributed fractures are infrequent in natural settings. As highlighted in Fig. 14(c), augmenting the fracture area by a factor of two folds enhanced non-uniformity within the formation flow. This results in increased gas injection and oil production rates for the case of upper injection, compared to that of the lower injection. Considering that oil predominantly flows within the tubing, while gas does through the annulus space, the method involving an upper injector is selected for further discussions in this study.

4.3. Effect of interlayer spacing

Layer spacing is one of the key parameters in radial borehole drilling design. Fig. 15 shows the relationship between oil production, gas storage, and time at a layer spacing ranging from 10 to 60 m. When layer spacing is lower than 20 m, the steady pressure stage (stage III) lasts for a very short time with gas channeling occurring immediately, and therefore both oil production rate and gas storage decrease with time. The oil production and gas storage rates are higher in the early stage when layer spacing is relatively small, but in the later stage decline faster than the case with a larger layer spacing. In the 10th year of production, cumulative oil production and gas storage increase first and then decrease with the increase of layer spacing. At a layer spacing of 20 m, both reach peak values of 2.56×10^4 t and 3.62×10^4 m^3, which are 1.97 and 1.84 times those at a layer spacing of 50 m, respectively.

When the pressure difference between the injector and producer remains constant, smaller layer spacing, meaning smaller flow distance between injector and producer, leads to a greater pressure gradient between two wells, making oil and gas flow more easily. Therefore, oil production and gas storage rates are higher when layer spacing is small, resulting in cumulative oil production and gas storage greater than other cases with larger layer spacing. However, in the 10th year, the ratio of produced gas over injected gas (R_g) and that of produced oil over injected gas (R_o) increase as layer spacing decreases. Wherein, the ratio R_o at a layer spacing of 10 m is 19.9 times that at a layer spacing of 20 m, as Fig. 16 shows. Such difference indicates large gas production that lowers oil production and gas storage efficiency at small layer spacing. In this case, declines in both rates are faster. Therefore, this paper selects 20 m as the optimal layer spacing based on cumulative oil production and cumulative gas storage. The subsequent discussion is based on 20 m layer spacing.

4.4. Effect of pressure difference

The pressure difference between injector and producer is the key parameter during production. Fig. 17 shows the changes in oil

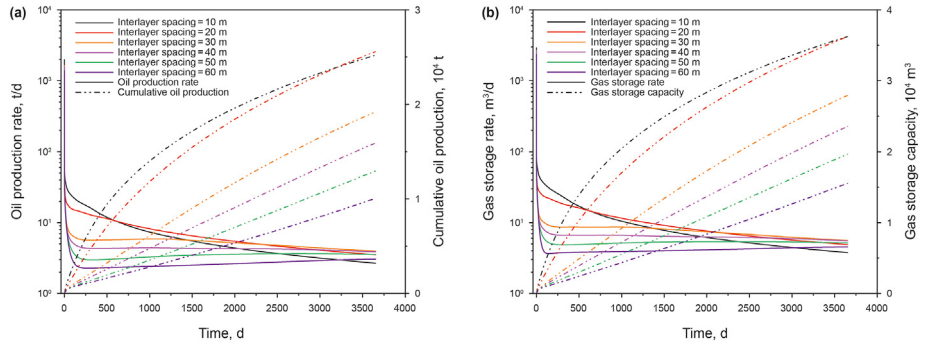

Fig. 15. Daily and cumulative production/storage vs. time at various interlayer spacing: (**a**) oil production (**b**) gas storage.

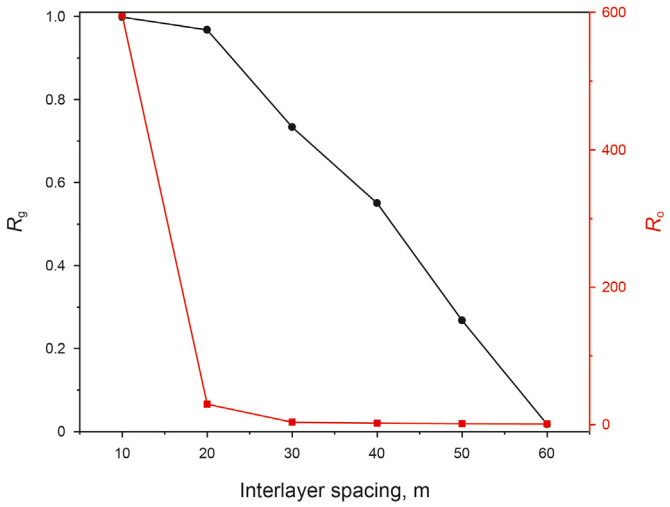

Fig. 16. Effect of interlayer spacing to R_g and R_o.

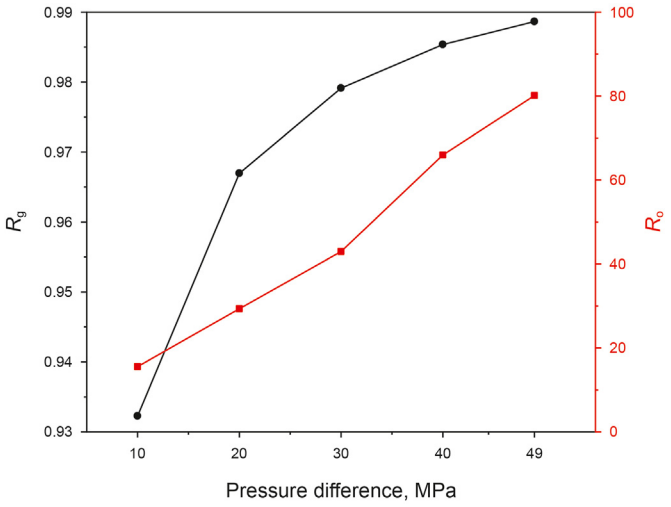

Fig. 18. Effect of pressure difference to R_g and R_o.

production and gas storage over time when the pressure difference is between 10 and 49 MPa. As is indicated in the figure, greater pressure difference leads to shorter steady production duration. In the early stage, greater pressure difference brings greater oil production and gas storage rates, yet so does the rate of decline in these values. In the 10th year, cumulative oil production and gas storage increase with increasing pressure difference, being 4.17×10^4 t and 5.57×10^4 m^3 at a pressure difference of 49 MPa, which are 1.64 and 1.55 times those at a pressure difference of 20 MPa, respectively.

Greater pressure difference leads to a greater pressure gradient between injector and producer, thus bringing greater fluid driving force, cumulative oil production, and gas storage. However, in the 10th year, R_g and R_o increase over increasing pressure difference, indicating increasing pressure difference will lower the efficiency of oil production and that of gas storage, as shown in Fig. 18.

4.5. Effect of borehole number

Borehole number is also one of the key parameters in radial borehole drilling design. Fig. 19 shows the relationship between oil production, gas storage, and time at borehole numbers ranging from 1 to 4. In the early stage, when the borehole number is large, oil production rate and gas storage rate are higher, but their rates of

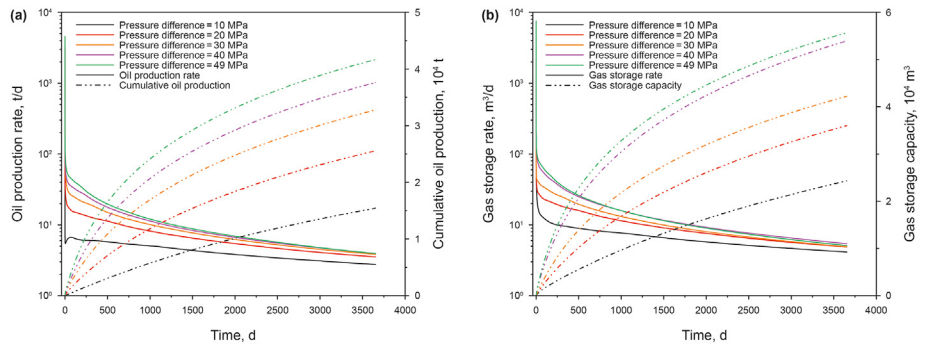

Fig. 17. Daily and cumulative production/storage vs. time at various pressure differences: (**a**) oil production (**b**) gas storage.

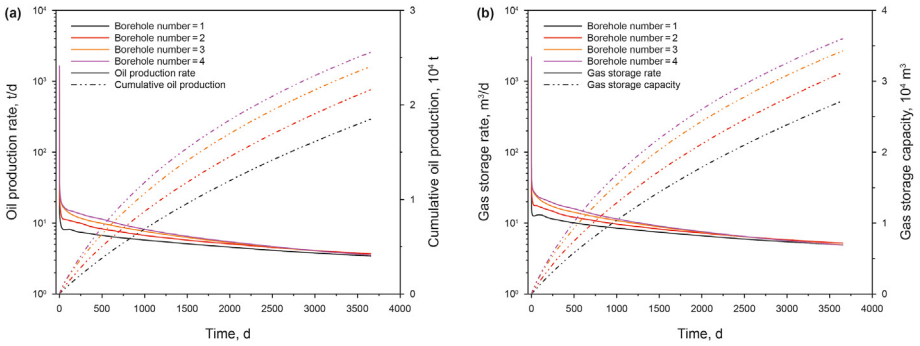

Fig. 19. Daily and cumulative production/storage vs. time at various borehole numbers: (**a**) oil production (**b**) gas storage.

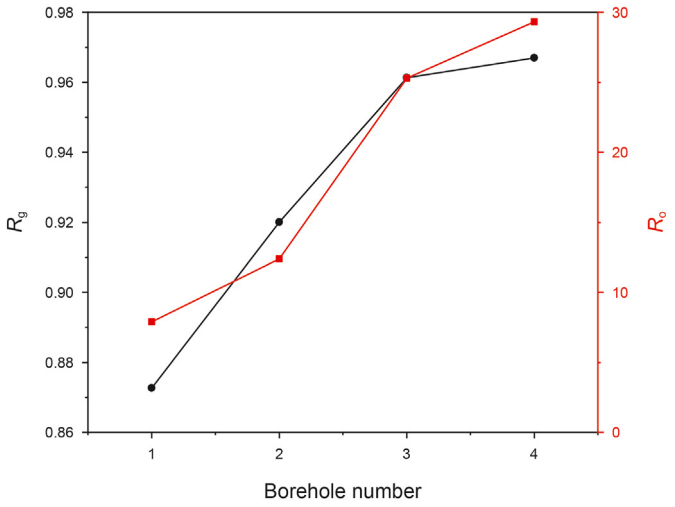

Fig. 20. Effect of borehole number to R_g and R_o.

decline are also faster than those with a smaller borehole number. In the 10th year, cumulative oil production and cumulative gas storage increase with increasing borehole number, but such a tendency slows down as borehole number continuously increases. Cumulative oil production and cumulative gas storage reach their peak values of 2.56×10^4 t and 3.62×10^4 m^3 at a borehole number of 4, which are 1.38 and 1.32 times the cases at a borehole number of 1.

More borehole numbers can induce more hydraulic fractures (this hypothesis, however, remains questionable when the borehole number is greater than 4). More hydraulic fractures will improve reservoir fluid mobility in both vertical and horizontal directions and therefore increase cumulative oil production and gas storage. In the 10th year, nonetheless, the two ratios R_g and R_o increase with an increasing borehole number, indicating more boreholes will lower the oil production and gas storage efficiency. Wherein, the ratio R_g and R_o at a borehole number of 4 are 1.11 and 3.72 times of those at a borehole number of 1, as shown in Fig. 20. Therefore, here a borehole number of 4 is selected as the optimal parameter, and subsequent discussion will be based on the case of 4 boreholes.

4.6. Effect of hydraulic fractures

Hydraulic fractures have the highest permeability in a reservoir and thereby will exert a significant influence on productivity. Fig. 21 shows the relationship between oil production, gas storage, and time at a fracture height ranging from 1 to 20 m. The duration of the steady production stage decreases with the increase of fracture height. In the 10th year of production, cumulative oil production and cumulative gas storage increase with increasing fracture height, while such a tendency declines as fracture height increases. Cumulative oil production and cumulative gas storage reach their peak values of 3.14×10^4 t and 4.42×10^4 m^3 at a fracture height of 20 m, which are 1.24 and 1.23 times those at a fracture height of 9 m.

Fig. 22 shows the relationship between oil production, gas storage, and time at a fracture length ranging from 50 to 150 m. In the 10th year of production, cumulative oil production and cumulative gas storage increase with increasing fracture length, while such tendency declines as fracture height continuously increases and reach the maximum at a fracture length of 150 m. The cumulative oil production and cumulative gas storage reach their peak values of 2.64×10^4 t and 3.70×10^4 m^3 at a fracture length of 150 m, which are 1.11 and 1.10 times the case at a fracture length of 75 m, but only 74.6 t and 78.0 m^3 differ from the case at a fracture height of 125 m.

An increase in hydraulic fracture height enhances the flow of reservoir fluid in the vertical direction, while an increase in

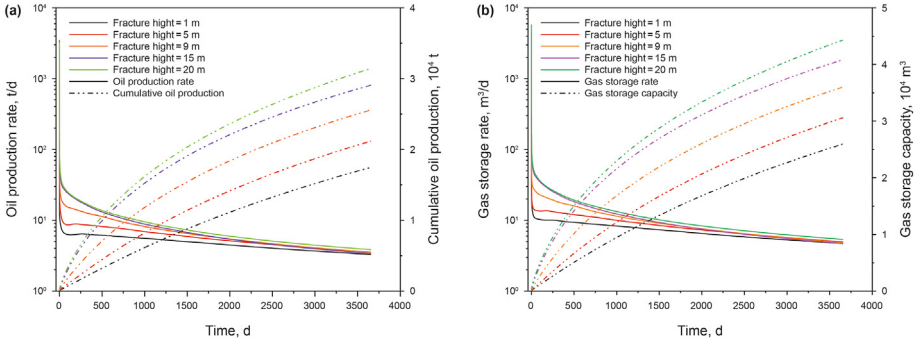

Fig. 21. Daily and cumulative production/storage vs. time at various fracture heights: (**a**) oil production (**b**) gas storage.

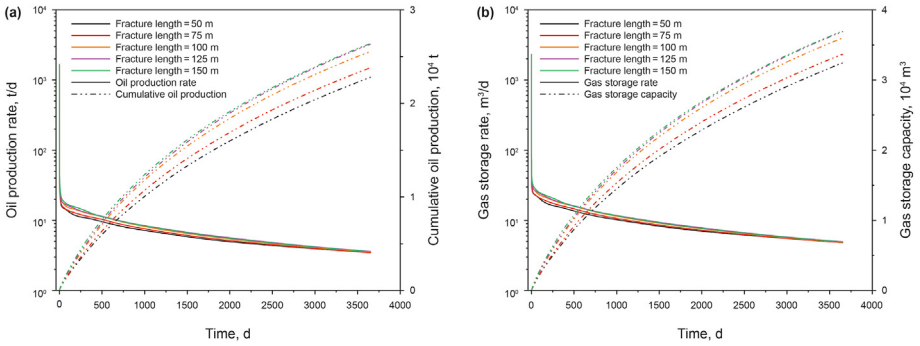

Fig. 22. Daily and cumulative production/storage vs. time at various fracture lengths: (**a**) oil production (**b**) gas storage.

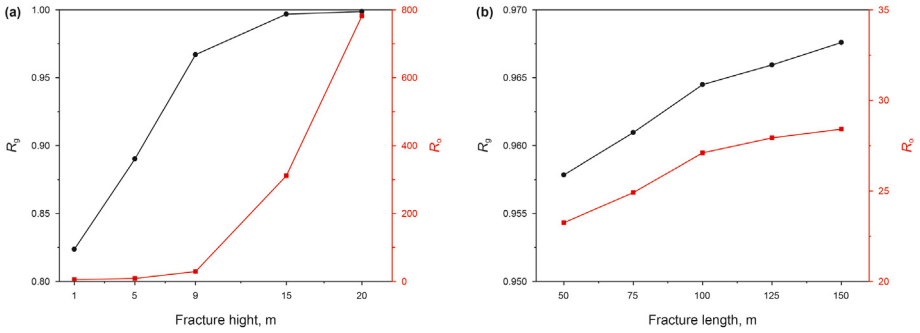

Fig. 23. Effect of (**a**) fracture height, and (**b**) fracture length to R_g and R_o.

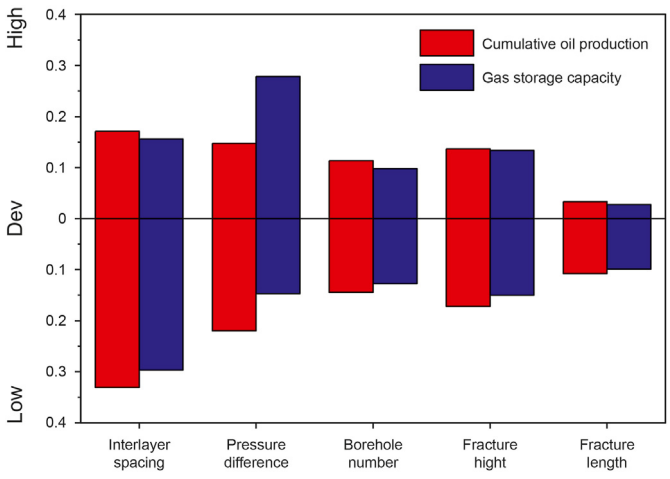

Fig. 24. Sensitivity analysis of parameters of CO_2 flooding with radial borehole fracturing ("High" represents the deviation caused by increasing the parameters. "Low" represents the deviation caused by increasing the parameters).

hydraulic fracture length enhances that in the horizontal direction, functioning similarly to the increase in borehole number. Although higher fractures bring more oil production and gas storage, R_g approaches 1, and that of R_o increases, as shown in Fig. 23. Wherein, R_g at a fracture height of 20 m is 26.68 times that at a fracture height of only 5 m. In contrast, fracture length exerts a smaller influence on ratios R_g and R_o.

4.7. Sensitivity analysis

Simulation results have shown influences caused by layer spacing, pressure difference, borehole number, and hydraulic fractures height and length on the productivity of the CO_2 flooding with radial borehole fracturing. The paper conducts a sensitivity analysis on these parameters based on the case with 20 m layer spacing, 30 MPa pressure difference, 2 boreholes, and hydraulic fractures 10 m in height, and 100 m in length. The analysis perturbs each parameter by ±50%. The sensitivity is quantified as the deviation of cumulative oil production and cumulative gas storage.

$$Dev_{\text{oil}} = \frac{sum_{\text{oil}} - sum_{\text{oil,base}}}{sum_{\text{oil,base}}} \tag{15}$$

$$Dev_{\text{gas}} = \frac{sum_{\text{gas}} - sum_{\text{gas,base}}}{sum_{\text{gas,base}}} \tag{16}$$

According to the sensitivity analysis in Fig. 24, the influence degree of parameters on cumulative oil production is as follows: layer spacing > pressure difference > hydraulic fracture height > borehole number > hydraulic fracture length. On the other hand, the influence degree of parameters on cumulative gas storage is as follows: pressure difference > layer spacing > hydraulic fracture height > borehole number > hydraulic fracture length. This result indicates that the main approach to increasing shale oil production and gas storage is to enhance shale oil vertical mobility.

5. Conclusions

To augment the oil recovery rate and CO_2 storage efficiency in shale reservoirs, this study introduces a novel development method predicated on the radial borehole fracture network, combined with CO_2 flooding. Drawing from parameters specific to the Gulong shale reservoir in China, a productivity model is established for a CO_2-flooded shale reservoir with radial borehole fracturing, grounded in the coupled matrix-fracture-wellbore flow

mechanism. Moreover, this study scrutinizes the relationships between reservoir pressure, CO_2 saturation, and time, and it delves into the impacts of CO_2 injection location, layer spacing, pressure difference, borehole number, and hydraulic fractures on productivity. Anticipated results could supply a theoretical foundation for efficiently exploiting shale reservoirs via radial borehole fracturing

- During production, four stages mark different production phases: pressure horizontal propagation stage, pressure vertical propagation stage, steady production stage, and gas channeling stage. The steady production stage and gas channeling stages mainly contribute to oil production and gas storage.
- The influence of CO_2 injection location on oil production and gas storage is negligible under a symmetric natural fractures distribution. However, given the usual field practices, this paper considers the upper CO_2 injector and lower oil producer to be the optimal configuration.
- Reduction in layer spacing can shorten the fluid migration distance and increase the pressure gradient between producer and injector (similar to the increase in pressure difference), thus improving oil production and gas storage significantly. Nonetheless, overly small layer spacing will cause severe gas channeling that lowers oil production and gas storage efficiency.
- When the radial borehole number is between 1 and 4, more boreholes can induce more hydraulic fractures and therefore improve fluid mobility in both horizontal and vertical directions, resulting in more oil production and gas storage.
- The main approach to increasing shale oil production and gas storage is to enhance shale oil vertical mobility, proving that the low vertical permeability in shale reservoirs is one of the main factors hindering production.
- CO_2 diffusion and adsorption are important factors affecting CO_2 flooding. The next work will further consider using component models to analyze the effects of CO_2 diffusion and adsorption. Moreover, the impact of the natural fractures and the stress sensitivity also need to be discussed.

Declaration of competing interest

We declare that we have no financial and personal relationships with other people or organizations that can inappropriately influence our work, there is no professional or other personal interest of any nature or kind in any product, service and/or company that could be construed as influencing the position presented in, or the review of, the manuscript entitled, "CO_2 Flooding in Shale Oil Reservoir with Radial Borehole Fracturing for CO_2 Storage and Enhanced Oil Recovery".

Acknowledgements

This study has been funded by the National Science Fund for Distinguished Young Scholars (No. 52204063) and Science Foundation of China University of Petroleum, Beijing (No. 2462023BJRC025). Moreover, we would like to express our heartfelt appreciation to the Computational Geosciences group in the Department of Mathematics and Cybernetics at SINTEF Digital for developing and providing the free open-source MATLAB Reservoir Simulation Toolbox (MRST) used in this research.

Appendix

In radial borehole fracturing, borehole pressure changes the stress field around the well. Each borehole guides one hydraulic fracture to propagate along the radial borehole direction and further along the maximum horizontal stress. Literature uses the guidance factor to describe the guidance effect of the radial borehole on hydraulic fractures (Guo et al., 2016), while in fact guidance factor can hardly describe the exact fracture created by radial borehole fracturing.

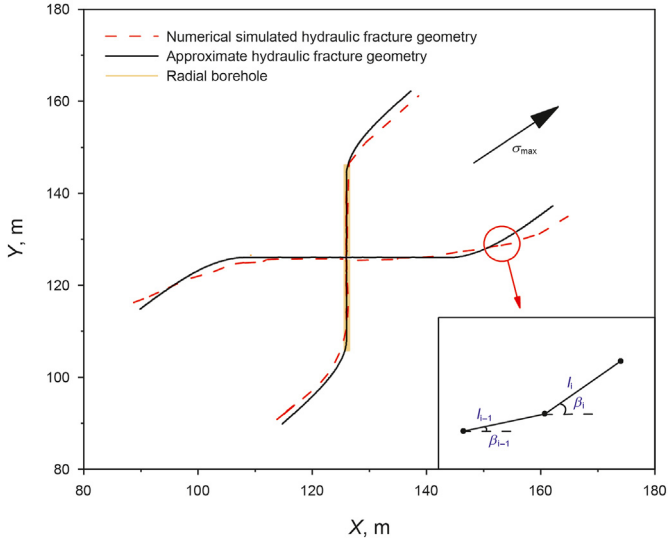

Fig. A1. Demonstration of hydraulic fracture distribution.

To approximate the shape of radial borehole in the horizontal direction, based on the numerical simulation results (Liu, 2019), this paper simplified the horizontal projection of fractures into several line segments connected end to end, as shown in Fig. A1 (top view). A line segment represents this part of hydraulic fracture morphology. The line segment then gradually deviates from the radial borehole, where the X and Y coordinate of the i-th line segment can be expressed as:

$$x_{P_i} = x_{main} + x_{P_{i-1}} + l_i \cos \beta_i \tag{A1}$$

$$y_{P_i} = y_{main} + y_{P_{i-1}} + l_i \sin \beta_i \tag{A2}$$

where x_{main} and y_{main} represent the X and Y coordinate of the main well in m; l_i represents the length of segment i in m; β_i represents the angle between the segment i and the minimum horizontal principal stress in °, and can be expressed as:

$$\beta_i = \beta_{i-1} + l_i \Delta\beta_i \tag{A3}$$

where $\Delta\beta_i$ represents angle change within unit length, expressed in °/m, and the larger the value is, the faster the fracture deviates to the direction of maximum horizontal principal stress. To describe the characteristic that the fracture tends to align with the maximum horizontal principal stress at long fracture propagation distance, $\Delta\beta_i$ is defined as:

$$\Delta\beta = \Delta\beta_0 \frac{\beta_{i-1} - \beta_{\sigma_{max}}}{\beta_{rb} - \beta_{\sigma_{max}}} \tag{A4}$$

where $\Delta\beta_0$ represents initial angle change within unit length, β_{rb} represents the angle of the radial borehole, and $\beta_{\sigma max}$ represents that of the maximum horizontal principal stress. Herein each fracture has a total length of 100 m, a height of 9 m. There are 5 line segments in total with $\Delta\beta_0$ being 0.3 °/m.

References

Abdel-Ghany, M.A., Siso, S., Hassan, A.M., Pierpaolo, P., Roberto, C., 2011. New Technology Application, Radial Drilling Petrobel, First Well in Egypt, Offshore Mediterranean Conference and Exhibition. OnePetro.

Alghalandis, Y.F., 2017. ADFNE: open source software for discrete fracture network engineering, two and three dimensional applications. Comput. Geosci. 102, 1–11. https://doi.org/10.1016/j.cageo.2017.02.002.
Bacon, D.H., Yonkofski, C.M., Schaef, H.T., White, M.D., McGrail, B.P., 2015. CO_2 storage by sorption on organic matter and clay in gas shale. J. Unconvent. Oil Gas Resour. 12, 123–133. https://doi.org/10.1016/j.juogr.2015.09.004.
Bai, Y., Liu, S.Q., Xia, Z.H., Chen, Y.X., Liang, G.Y., Shen, Y., 2021. Fracture initiation mechanisms of multibranched radial-drilling fracturing. Lithosphere 2021 (1), 3316083. https://doi.org/10.2113/2021/3316083.
Bai, G., Su, J., Li, X.M., Guo, C.S., Han, M.X., Zhou, X.H., 2022. Step-by-step CO_2 injection pressure for enhanced coal seam gas recovery: a laboratory study. Energy 260, 125197. https://doi.org/10.1016/j.energy.2022.125197.
Boak, J., Kleinberg, R., 2020. Shale gas, tight oil, shale oil and hydraulic fracturing. Future Energy. Elsevier 67–95. https://doi.org/10.1016/B978-0-08-102886-5.00004-9.
Cavanagh, A., Ringrose, P., 2014. Improving oil recovery and enabling CCS: a comparison of offshore gas-recycling in Europe to CCUS in North America. Energy Proc. 63, 7677–7684. https://doi.org/10.1016/j.egypro.2014.11.801.
Cinelli, S.D., Kamel, A.H., 2013. Novel technique to drill horizontal laterals revitalizes aging field. In: SPE/IADC Drilling Conference. OnePetro. https://doi.org/10.2118/163405-MS.
Cui, G.D., Wang, W.X., Dou, B., Liu, Y.F., Tian, H., Zheng, J., et al., 2022. Geothermal energy exploitation and power generation via a single vertical well combined with hydraulic fracturing. J. Energy Eng. 148 (1), 04021058. https://doi.org/10.1061/(ASCE)EY.1943-7897.0000809.
Dachanuwattana, S., Jin, J.L., Zuloaga-Molero, P., Li, X.L., Xu, Y.F., Sepehrnoori, K., et al., 2018. Application of proxy-based MCMC and EDFM to history match a Vaca Muerta shale oil well. Fuel 220, 490–502. https://doi.org/10.1016/j.fuel.2018.02.018.
Dai, J.C., Wang, T.Y., Tian, K.J., Weng, J.T., Li, J.B., Li, G.S., 2023a. CO_2 huff-n-puff combined with radial borehole fracturing to enhance oil recovery and store CO_2 in a shale oil reservoir. Geoenergy Sci. Eng., 212012 https://doi.org/10.1016/j.geoen.2023.212012.
Dai, J.C., Zheng, Z.Y., Wang, T.Y., Li, G.S., 2023b. Productivity and cost comparison between radial-borehole fracturing and horizontal well fracturing in shale oil reservoir. In: Gas & Oil Technology Showcase and Conference. OnePetro. https://doi.org/10.2118/214197-MS.
Du, J.H., Hu, S.Y., Pang, Z.L., Lin, S.H., Hou, L.H., Zhu, R.K., 2019. The types, potentials and prospects of continental shale oil in China. China Petrol. Explor. 24 (5), 560. https://doi.org/10.3969/j.issn.1672-7703.2019.05.003.
Gamadi, T.D., Sheng, J.J., Soliman, M.Y., Menouar, H., Watson, M.C., Emadibaladehi, H., 2013. An Experimental Study of Cyclic Gas Injection to Improve Shale Oil Recovery, SPE Annual Technical Conference and Exhibition. OnePetro. https://doi.org/10.2118/169142-MS.
Gong, D.G., Qu, Z.Q., Guo, T.K., Tian, Y., Tian, K.H., 2016. Variation rules of fracture initiation pressure and fracture starting point of hydraulic fracture in radial well. J. Petrol. Sci. Eng. 140, 41–56. https://doi.org/10.1016/j.petrol.2016.01.006.
Guo, T.K., Qu, Z.Q., Gong, D.G., Lei, X., Liu, M., 2016. Numerical simulation of directional propagation of hydraulic fracture guided by vertical multi-radial boreholes. J. Nat. Gas Sci. Eng. 35, 175–188. https://doi.org/10.1016/j.jngse.2016.08.056.
Guo, T.K., Qu, Z.Q., Gong, F.C., Wang, X.Z., 2017. Numerical simulation of hydraulic fracture propagation guided by single radial boreholes. Energies 10 (10), 1680. https://doi.org/10.3390/en10101680.
Guo, Z.Q., Tian, S.C., Liu, Q.L., Ma, L.Y., Yong, Y.N., Yang, R.Y., 2022. Experimental investigation on the breakdown pressure and fracture propagation of radial borehole fracturing. J. Petrol. Sci. Eng. 208, 109169. https://doi.org/10.1016/j.petrol.2021.109169.
Hoffman, B.T., 2012. In: Comparison of Various Gases for Enhanced Recovery from Shale Oil Reservoirs, SPE Improved Oil Recovery Symposium. OnePetro. https://doi.org/10.2118/154329-MS.
Hu, S.Y., Zhao, W.Z., Hou, L.H., Yang, Z., Zhu, R.K., Wu, S.T., et al., 2020. Development potential and technical strategy of continental shale oil in China. Petrol. Explor. Dev. 47 (4), 877–887. https://doi.org/10.1016/S1876-3804(20)60103-3.
Huang, Z., Huang, Z.W., 2019. Review of radial jet drilling and the key issues to be applied in new geo-energy exploitation. Energy Proc. 158, 5969–5974. https://doi.org/10.1016/j.egypro.2019.01.524.
Huang, J.W., Jin, T.Y., Barrufet, M., Killough, J., 2020. Evaluation of CO_2 injection into shale gas reservoirs considering dispersed distribution of kerogen. Appl. Energy 260, 114285. https://doi.org/10.1016/j.apenergy.2019.114285.
Jia, B., Tsau, J.S., Barati, R., 2019. A review of the current progress of CO_2 injection EOR and carbon storage in shale oil reservoirs. Fuel 236, 404–427. https://doi.org/10.1016/j.fuel.2018.08.103.
Jin, L., Hawthorn, S., Sorensen, J., Pekot, L., Kurz, B., Smith, S., et al., 2017. Advancing CO_2 enhanced oil recovery and storage in unconventional oil play—experimental studies on Bakken shales. Appl. Energy 208, 171–183. https://doi.org/10.1016/j.apenergy.2017.10.054.
Kim, J.G., Deo, M.D., 2000. Finite element, discrete-fracture model for multiphase flow in porous media. AIChE J. 46 (6), 1120–1130. https://doi.org/10.1002/aic.690460604.
Lan, D.J., Lun, Z.M., Lyu, C.Y., Wang, H.T., Zhao, Q.M., Sheng, H., 2021. Nuclear magnetic resonance experimental study of CO_2 injection to enhance shale oil recovery. Petrol. Explor. Dev. 48 (3), 702–712. https://doi.org/10.1016/S1876-3804(21)60056-3.
Lee, S.H., Jensen, C.L., Lough, M.F., 2000. Efficient finite-difference model for flow in a reservoir with multiple length-scale fractures. SPE J. 5 (3), 268–275. https://doi.org/10.2118/65095-PA.
Lee, S.H., Lough, M.F., Jensen, C.L., 2001. Hierarchical modeling of flow in naturally fractured formations with multiple length scales. Water Resour. Res. 37 (3), 443–455. https://doi.org/10.1029/2000WR900340.
Lei, Q., Weng, D.W., Xiong, S.C., Liu, H.B., Guan, B.S., Deng, Q., et al., 2021. Progress and development directions of shale oil reservoir stimulation technology of China National Petroleum Corporation. Petrol. Explor. Dev. 48 (5), 1198–1207. https://doi.org/10.1016/S1876-3804(21)60102-7.
Li, Y.H., Wang, C.J., Shi, L.H., Guo, W.Y., 2000. Application and development of drilling and completion of the ultrashort-radius radial well by high pressure jet flow techniques. International Oil and Gas Conference and Exhibition in China. OnePetro. https://doi.org/10.2118/64756-MS.
Li, L., Zhang, Y., Sheng, J.J., 2017. Effect of the injection pressure on enhancing oil recovery in shale cores during the CO_2 huff-n-puff process when it is above and below the minimum miscibility pressure. Energy Fuel. 31 (4), 3856–3867. https://doi.org/10.1021/acs.energyfuels.7b00031.
Li, X.L., Zhang, R.S., Qu, Z.Q., 2019. Research on the crack morphology of radial well fracturing. International Field Exploration and Development Conference. Springer, pp. 2707–2720.
Li, Y.W., Long, M., Tang, J.Z., Chen, M., Fu, X.F., 2020. A hydraulic fracture height mathematical model considering the influence of plastic region at fracture tip. Petrol. Explor. Dev. 47 (1), 184–195. https://doi.org/10.1016/S1876-3804(20)60017-9.
Lie, K.A., 2019. An Introduction to Reservoir Simulation Using MATLAB/GNU Octave: User Guide for the MATLAB Reservoir Simulation Toolbox (MRST). Cambridge University Press.
Lie, K.A., Møyner, O., 2021. Advanced Modelling with the MATLAB Reservoir Simulation Toolbox. Cambridge University Press.
Liu, Q.L., 2019. Study on Fracturing Control Mechanism and Parameter Optimization by Radial Jet Drilling with Hydraulic Fracturing. China University of Petroleum (Beijing). Chinese, Diss.
Liu, H.J., Were, P., Li, Q., Gou, Y., Hou, Z., 2017. Worldwide status of CCUS technologies and their development and challenges in China. Geofluids 2017. https://doi.org/10.1155/2017/6126505.
Liu, Q.L., Tian, S.C., Li, G.S., Sheng, M., Li, X.J., Wang, T.Y., et al., 2018. An analytical model for fracture initiation from radial lateral borehole. J. Petrol. Sci. Eng. 164, 206–218. https://doi.org/10.1016/j.petrol.2018.01.056.
Liu, C.X., Gupta, A., Yu, W., Vaidya, N.N., Li, N., Sepehrnoori, K., 2021. Characterization of hydraulic fracture properties in Eagle Ford shale oil reservoir using EDFM-AI with two fracture design scenarios. In: Unconventional Resources Technology Conference, 26–28 July 2021. Unconventional Resources Technology Conference (URTeC), pp. 1851–1866. https://doi.org/10.15530/urtec-2021-5381.
Moinfar, A., Varavei, A., Sepehrnoori, K., Johns, R.T., 2013. Development of a coupled dual continuum and discrete fracture model for the simulation of unconventional reservoirs. In: SPE Reservoir Simulation Symposium. OnePetro. https://doi.org/10.2118/163647-MS.
Mukherjee, H., Economides, M.J., 1991. A parametric comparison of horizontal and vertical well performance. SPE Form. Eval. 6 (2), 209–216. https://doi.org/10.2118/18303-PA.
Novokreshchennykh, D.V., Raspopov, A.V., 2016. Efficiency of radial drilling and acidizing technologies in carbonate reservoirs of Perm Region (Russian). Neftyanoe khozyaystvo-Oil Industry 2016 (4), 118–121.
Pang, Y.M., Wang, Y.Z., Wang, R., Zhang, Y.Q., Lu, H.M., Huang, L., 2020. Production test analysis and productivity prediction of horizontal wells in Gulong shale oil reservoirs, Songliao Basin. Pet. Geol. Oilfield Dev. Daqing 39 (3), 137–146. https://doi.org/10.19597/J.ISSN.1000-3754.202005004 (in Chinese).
Peaceman, D.W., 1983. Interpretation of well-block pressures in numerical reservoir simulation with nonsquare grid blocks and anisotropic permeability. Soc. Petrol. Eng. J. 23 (3), 531–543. https://doi.org/10.2118/10528-PA.
Sheng, J.J., 2015. Enhanced oil recovery in shale reservoirs by gas injection. J. Nat. Gas Sci. Eng. 22, 252–259. https://doi.org/10.1016/j.jngse.2014.12.002.
Sheng, J.J., Chen, K., 2014. Evaluation of the EOR potential of gas and water injection in shale oil reservoirs. J. Unconvent. Oil Gas Resour. 5, 1–9. https://doi.org/10.1016/j.juogr.2013.12.001.
Shi, Y., Song, X.Z., Shen, Z.H., Wang, G.S., Li, X.J., Zheng, R., et al., 2018. Numerical investigation on heat extraction performance of a CO_2 enhanced geothermal system with multilateral wells. Energy 163, 38–51. https://doi.org/10.1016/j.energy.2018.08.060.
Simpson, M.D., Patterson, R., Wu, K., 2016. Study of stress shadow effects in Eagle Ford shale: insight from field data analysis. In: 50th US Rock Mechanics/Geomechanics Symposium. OnePetro.
Song, C.Y., Yang, D.Y., 2017. Experimental and numerical evaluation of CO_2 huff-n-puff processes in Bakken formation. Fuel 190, 145–162. https://doi.org/10.1016/j.fuel.2016.11.041.
Sorensen, J.A., Pekot, L.J., Torres, J.A., Jin, L., Hawthorne, S.B., Smith, S.A., et al., 2018. Field test of CO_2 injection in a vertical middle Bakken well to evaluate the potential for enhanced oil recovery and CO_2 storage. In: SPE/AAPG/SEG Unconventional Resources Technology Conference. OnePetro. https://doi.org/10.15530/urtec-2018-2902813.
Sun, L.D., Liu, H., He, W.Y., Li, G.X., Zhang, S.C., Zhu, R.K., et al., 2021. An analysis of major scientific problems and research paths of Gulong shale oil in Daqing Oilfield, NE China. Petrol. Explor. Dev. 48 (3), 527–540. https://doi.org/10.1016/S1876-3804(21)60043-5.

Tang, J.Z., Wu, K., Zuo, L.H., Xiao, L.Z., Sun, S.J., Ehlig-Economides, C., 2019. Investigation of rupture and slip mechanisms of hydraulic fractures in multiple-layered formations. SPE J. 24 (5), 2292–2307. https://doi.org/10.2118/197054-PA.

Teng, X.Q., Yang, P., Li, N., Yang, C.X., Jin, Y., Lu, Y.H., et al., 2014. Radial drilling revitalizes aging field in Tarim: a case study. In: SPE/ICoTA Coiled Tubing and Well Intervention Conference and Exhibition. OnePetro. https://doi.org/10.2118/168282-MS.

Tian, Y., Qu, Z.Q., Guo, T.K., Tian, Y.Y., 2017. Theoretical research on radial wells orientating hydraulically created fracture directional extended. Int. J. Hydrogen Energy 42 (29), 18358–18363. https://doi.org/10.1016/j.ijhydene.2017.04.179.

Tian, S.C., Huang, Z.W., Li, G.S., Lu, P.Q., Zhang, H.Y., Wang, T.Y., 2019. Laboratory experiments on blockage removing and stimulation of CBM reservoirs by composite pulsating hydraulic fracturing of radial horizontal wells. Nat. Gas. Ind. B 6 (2), 151–158. https://doi.org/10.1016/j.ngib.2018.09.005.

Wang, X.K., Sheng, J.J., 2017. Effect of low-velocity non-Darcy flow on well production performance in shale and tight oil reservoirs. Fuel 190, 41–46. https://doi.org/10.1016/j.fuel.2016.11.040.

Wang, T.Y., Liu, Q.L., Zhu, B., Tian, S.C., Li, G.S., Guo, Z.Q., 2020. Fracture initiation characteristics from multiple radial wellbores. 54th US Rock Mechanics/Geomechanics Symposium. OnePetro.

Wang, Z.Y., Zhao, X.L., Xiong, S.C., He, Y., 2021. Semi-analytical model-based research on influencing factors of the spacing of volume fracturing horizontal well in tight oil reservoirs via consideration of imbibition. J. Petrol. Sci. Eng. 198, 108167. https://doi.org/10.1016/j.petrol.2020.108167.

Xie, Y.C., Hou, Z.M., Liu, H.J., Cao, C., Qi, J.G., 2021. The sustainability assessment of CO_2 capture, utilization and storage (CCUS) and the conversion of cropland to forestland program (CCFP) in the Water–Energy–Food (WEF) framework towards China's carbon neutrality by 2060. Environ. Earth Sci. 80 (14), 1–17.

Xu, Y.F., 2015. Implementation and Application of the Embedded Discrete Fracture Model (EDFM) for Reservoir Simulation in Fractured Reservoirs. The University of Texas at Austin, Diss.

Xu, L., Li, Q., Myers, M., Chen, Q., Li, X.C., 2019. Application of nuclear magnetic resonance technology to carbon capture, utilization and storage: a review. J. Rock Mech. Geotech. Eng. 11 (4), 892–908. https://doi.org/10.1016/j.jrmge.2019.01.003.

Yan, C.L., Cheng, Y.F., Deng, F.C., Liang, Q.M., Teng, F., Li, Q.C., 2017. Experimental study on the hydraulic fracturing of radial horizontal wells. 4th ISRM Young Scholars Symposium on Rock Mechanics. OnePetro.

Yang, G.F., Zhou, Q.F., Lu, X.M., 2019. Study on the cost of shale oil exploration and development. China Petrol. Explor. 24 (5), 576. https://doi.org/10.3969/j.issn.1672-7703.2019.05.005 (in Chinese).

Yang, R.Y., Li, G.S., Qin, X.Z., Huang, Z.W., Li, J.B., Sheng, M., et al., 2022. Productivity enhancement in multilayered coalbed methane reservoirs by radial borehole fracturing. Petrol. Sci. 19 (6), 2844–2866. https://doi.org/10.1016/j.petsci.2022.06.019.

Zeng, H., Jin, Y., Wang, D.B., Yu, B., Zhang, W., 2022. Numerical simulation on hydraulic fracture height growth across layered elastic–plastic shale oil reservoirs. Processes 10 (8), 1453. https://doi.org/10.3390/pr10081453.

Zhao, X.Z., Zhou, L.H., Pu, X.G., Jin, F.M., Han, W.Z., Xiao, D.Q., et al., 2018. Geological characteristics of shale rock system and shale oil exploration breakthrough in a lacustrine basin: a case study from the Paleogene 1st sub-member of Kong 2 Member in Cangdong Sag, Bohai Bay Basin, China. Petrol. Explor. Dev. 45 (3), 377–388. https://doi.org/10.1016/S1876-3804(18)30043-0.

Zhao, X., Ma, X.W., Chen, B.Y., Shang, Y.P., Song, M.L., 2022. Challenges toward carbon neutrality in China: strategies and countermeasures. Resour. Conserv. Recycl. 176, 105959. https://doi.org/10.1016/j.resconrec.2021.105959.

Zhu, C.F., Sheng, J.J., Ettehadtavakkol, A., Li, Y.J., Gong, H.J., Li, Z.J., et al., 2019. Numerical and experimental study of enhanced shale-oil recovery by CO_2 miscible displacement with NMR. Energy Fuel. 34 (2), 1524–1536. https://doi.org/10.1021/acs.energyfuels.9b03613.

Zou, C.N., Yang, Z., Zhu, R.K., Zhang, G.S., Hou, L.H., Wu, S.T., et al., 2015. Progress in China's unconventional oil & gas exploration and development and theoretical technologies. Acta Geologica Sinica-English Edition 89 (3), 938–971. https://doi.org/10.1111/1755-6724.12491.